Developmental Cell
Article

Rif1 Maintains Telomere Length Homeostasis of ESCs by Mediating Heterochromatin Silencing

Jiameng Dan,[1,6] Yifei Liu,[2,6] Na Liu,[1,6] Maria Chiourea,[3] Maja Okuka,[4] Tao Wu,[2] Xiaoying Ye,[1] Chunlin Mou,[1] Lei Wang,[1] Lingling Wang,[1] Yu Yin,[1] Jihong Yuan,[1] Bingfeng Zuo,[1] Fang Wang,[1] Zhiguo Li,[1] Xinghua Pan,[2] Zhinan Yin,[1] Lingyi Chen,[1] David L. Keefe,[5] Sarantis Gagos,[3] Andrew Xiao,[2,*] and Lin Liu[1,*]
[1]State Key Laboratory of Medicinal Chemical Biology, Department of Cell Biology and Genetics, College of Life Sciences, Nankai University, Tianjin 300071, China
[2]Yale Stem Cell Center and Department of Genetics, Yale University School of Medicine, New Haven, CT 06519, USA
[3]Laboratory of Genetics, Center of Basic Research II, Biomedical Research Foundation of the Academy of Athens Greece (BRFAA), Soranou Efesiou 4, Athens 11527, Greece
[4]Department of Obstetrics and Gynecology, University of South Florida College of Medicine, Tampa, FL 33612, USA
[5]Department of Obstetrics and Gynecology, New York University Langone Medical Center, New York, NY 10016, USA
[6]Co-first authors
*Correspondence: andrew.xiao@yale.edu (A.X.), liulin@nankai.edu.cn (L.L.)
http://dx.doi.org/10.1016/j.devcel.2014.03.004

SUMMARY

Telomere length homeostasis is essential for genomic stability and unlimited self-renewal of embryonic stem cells (ESCs). We show that telomere-associated protein Rif1 is required to maintain telomere length homeostasis by negatively regulating *Zscan4* expression, a critical factor for telomere elongation by recombination. Depletion of *Rif1* results in terminal hyperrecombination, telomere length heterogeneity, and chromosomal fusions. Reduction of *Zscan4* by shRNA significantly rescues telomere recombination defects of *Rif1*-depleted ESCs and associated embryonic lethality. Further, Rif1 negatively modulates *Zscan4* expression by maintaining H3K9me3 levels at subtelomeric regions. Mechanistically, Rif1 interacts and stabilizes H3K9 methylation complex. Thus, *Rif1* regulates telomere length homeostasis of ESCs by mediating heterochromatic silencing.

INTRODUCTION

Telomere-associated protein Rif1 was originally identified in budding yeast as a RAP1 interacting factor 1 that negatively regulates telomere length (Hardy et al., 1992). Rif1 plays an important role in yeast telomere length homeostasis by regulating telomerase recruitment to telomeres (Levy and Blackburn, 2004; Teixeira et al., 2004) or by stabilizing Rap1 in conjunction with Rif2 (Shi et al., 2013). Rif1 is also involved in repression of TERRA transcription (Iglesias et al., 2011). Rif1 has been recently shown to play roles in the DNA damage response and replication timing regulation in differentiated mammalian cells (Buonomo et al., 2009; Callen et al., 2013; Chapman et al., 2013; Cornacchia et al., 2012; Di Virgilio et al., 2013; Escribano-Díaz et al., 2013; Silverman et al., 2004; Wang et al., 2009; Xu and Blackburn, 2004; Yamazaki et al., 2012; Zimmermann et al., 2013). In addition, *Rif1* deficiency in vivo leads to embryonic lethality in mice (Buonomo et al., 2009), suggesting that Rif1 is critical for early embryo development.

Thus far, no evidence has been found for a role of mammalian *Rif1* ortholog in telomere length regulation. It is interesting that *Rif1* is highly expressed in mouse embryonic stem cells (ESCs) and germ cells (Adams and McLaren, 2004; Hu et al., 2009). *Rif1* also is a target of Oct4, Sox2, and Nanog in ESCs and implicated in ES self-renewal (Loh et al., 2006; Wang et al., 2006), but the function of *Rif1* in ESCs remains elusive. In an attempt to understand the roles of *Rif1* in ESC self-renewal and pluripotency and the underlying mechanisms, we found that *Rif1* is required to maintain telomere length homeostasis and genomic stability of ESCs by facilitating heterochromatin silencing at subtelomeres to prevent overexpression of Zscan4, a critical factor that controls telomere recombination (Zalzman et al., 2010).

RESULTS

Depletion of *Rif1* Impairs Cell Proliferation and Pluripotency of ESCs

We confirmed that *Rif1* was highly expressed in ESCs and testis, while its expression level was very low in mouse embryonic fibroblasts (MEF) and various somatic tissues (Figures 1A and 1B), implying that Rif1 may play important roles in ESCs and early development. To understand the role of *Rif1* in ESCs, we established *Rif1* knockdown (KD) cell lines by RNA interference using at least two shRNA constructs (Figure S1A available online; Supplemental Experimental Procedures) and assessed the capacity for proliferation, differentiation, and pluripotency of ESCs. The mRNA and protein levels of *Rif1* were effectively reduced to about 20% of controls, similar to those of MEF (Figures 1C and 1D). Cell proliferation was reduced in stable *Rif1* KD cells (Figure 1E; Figure S1B), consistent with reduced 5′-bromo-2′-deoxyuridine (BrdU) incorporation (Figures S1C and S1D). Also, *Rif1*-depleted cells after long-term culture (passage number >20) showed markedly increased expression of genes associated with cellular senescence, particularly p16 (*INK4a*) and p21 (*Cip1*) (Bringold and Serrano, 2000; Herbig et al., 2004) (Figure S1E). Consistently, long-term culture of *Rif1* KD cells also

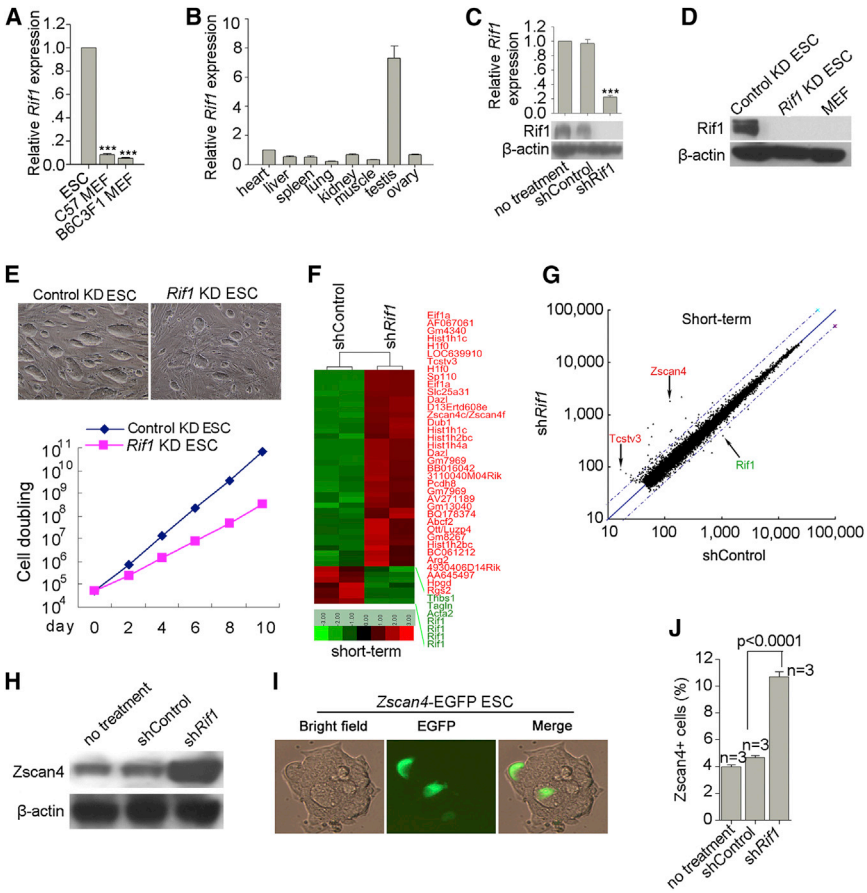

Figure 1. *Rif1* Is Required for ESC Self-Renewal and Negatively Regulates Expression of *Zscan4*

(A) Relative *Rif1* expression levels in ESCs and MEFs.

(B) *Rif1* expression levels in various mouse tissues by qPCR analysis.

(C) KD efficiency of *Rif1* by transient shRNA confirmed by qPCR and western blot.

(D) Very low Rif1 protein level in *Rif1* stable KD ESCs by western blot, comparable to that of MEFs.

(E) Reduced clonal size and cell proliferation of ESCs (F1 of B6C3F1 background) resulting from stable *Rif1* KD following 24 passages.

(F) Heat map cluster showing genes that are differentially expressed (FDR $\leq$ 0.05, and fold $\geq$ 2.0) following transient *Rif1* KD by shRNA for 48 hr, compared to control shRNA.

(G) Scatterplot showing differentially expressed genes (FDR $\leq$ 0.05, and fold $\geq$ 2.0) following transient *Rif1* KD.

(H) Elevated Zscan4 protein level following *Rif1* KD for 48 hr by shRNA shown by western blot.

(I) Expression pattern of *Zscan4* in J1 ESCs visualized by EGFP reporter (green), showing only a subset of ESCs expressing *Zscan4* at a given time.

(J) *Rif1* transient KD increases Zscan4-EGFP positive cells by FACS.

Error bars indicate mean ± SEM (n = 3). ***p < 0.001 by ANOVA and PLSD analysis. See also Figures S1 and S2.

led to senescence-associated β-galactosidase (SA-β-gal) expression, a marker for senescence (Figures S1F and S1G). Of note, the increased expression of senescence-associated genes and SA-β-gal staining were most likely due to indirect effects of long-term cell culture, since we did not find such upregulation in the short-term *Rif1* KD cells.

In addition, expression of pluripotency genes, such as *Oct4*, was reduced in stable *Rif1* KD cells (Figures S1H and S1I). In vitro embryoid body formation assay showed that *Rif1* KD impaired differentiation of ESCs toward the neural lineage, as indicated by βIII-tubulin staining. However, *Rif1* deficiency did not seem to affect differentiation toward the endoderm lineage (as indicated by α-fetoprotein staining) and mesoderm lineage (as indicated by α-smooth muscle actin staining) (Figure S1J). Notably, stable *Rif1* KD ESCs produced neither teratomas by injection under the skin of immunodeficient mice (Figure S1K) nor chimeras by injection into albino recipient embryos, in contrast to control KD ESCs (Figure S1L). These data strongly argue that Rif1 is essential for early embryogenesis and pluripotency of ESCs.

Rif1 Negatively Regulates Expression of *Zscan4*

To understand the mechanisms underlying *Rif1* function in ESCs and early embryogenesis, we performed global gene expression analysis of *Rif1* stable KD ESC lines (more than ten passages) using Affymetrix 430 2.0 arrays. More genes were upregulated than downregulated in ESCs following *Rif1* depletion, compared to KD controls (Table S1; Figures S2A–S2C). Among those genes, *Zscan4*, together with *Tcstv1* and *Tcstv3*, which are specific to early two-cell-stage embryos and ESCs (Falco et al., 2007; Zalzman et al., 2010; Zhang et al., 2006), were highly upregulated in *Rif1*-depleted ESCs (Figures S2A and S2B).

A selected group of genes that showed differential expression by microarray was verified by quantitative real-time PCR analysis in two additional ESC lines (Figure S2D). Also, Zscan4 protein levels were significantly elevated in *Rif1* KD ESCs, compared to control KD ESCs, and were minimal in MEF, by western blot analysis (Figure S2E). Changes in expression of these genes could result from indirect effects caused by *Rif1* depletion. Thus, we further generated and analyzed the global gene expression in transient *Rif1* KD (48 hr after KD) ESCs (Figures 1F and 1G; Table S2). Consistently, *Zscan4*, *Tcstv3*, and an additional gene, *Eif1α,* specific to two-cell embryos, showed rapid upregulation following transient KD of *Rif1* (Figures 1F and 1G). Quantitative PCR analysis of two ESC lines with different genetic background also confirmed the microarray data (Figures S2F and S2G). Similar expression profile was achieved in ESCs using another *Rif1* KD construct (shRNA-2) (Figure S2G), indicating that the gene expression changes were specific to *Rif1* depletion. Increased protein levels of Zscan4 by *Rif1* KD were confirmed by immunoblot (Figure 1H). Both *Zscan4* and *Rif1* mRNA and protein levels were high in ESCs but extremely low or undetectable in somatic cells, such as MEF, and several types of tissues (Figure 1; Figure S2E). Global gene expression analysis

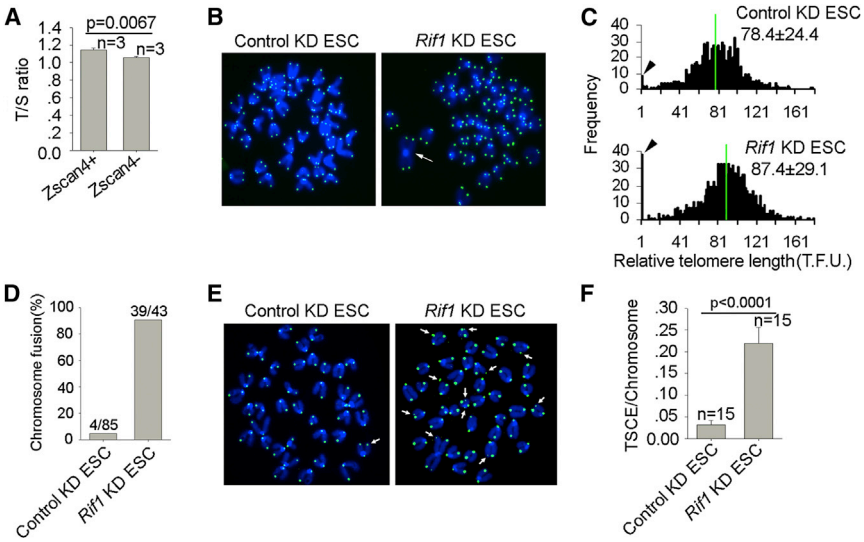

Figure 2. *Rif1* Regulates Telomere Length Homeostasis in ESCs

(A) Longer telomeres in *Zscan4*-positive than in *Zscan4*-negative cells by qPCR.

(B) Clonal chromosome fusion (arrow) in *Rif1* KD ESCs (ESC) shown by telomere-specific PNA-FISH.

(C) Distribution histogram of relative telomere length in *Rif1* KD ESCs analyzed by telomere Q-FISH and TFL-TELO software. Green lines indicate median telomere length. The average length ± SD is given in the upper right corner. Arrowheads indicate frequency of telomere loss.

(D) Increased frequency of chromosomal terminal fusions by *Rif1* KD.

(E) Micrographs showing T-SCE (arrows) by CO-FISH analysis.

(F) Increased frequency of T-SCE per chromosome by *Rif1* KD. Statistical comparison made by Mann-Whitney test.

See also Figure S3.

showed that genes upregulated in *Rif1* transient KD ESCs mostly overlapped with those of *Rif1* stable KD ESCs.

To determine whether depletion of *Rif1* increases the proportion of *Zscan4*$^+$ ESCs at any given time, we generated a *Zscan4* promoter-driven EGFP (*Zscan4*-EGFP) ESC line. We transiently knocked down *Rif1* and sorted ESCs into *Zscan4*$^+$ and *Zscan4*$^-$ populations by flow cytometry (Figure 1I; Figure S2H). Consistent with a recent report (Zalzman et al., 2010), *Zscan4* was expressed in only about 5% of control KD ESCs at any given time. However, *Rif1* KD doubled the percentage of *Zscan4*$^+$ ESCs (Figure 1J). Higher expression levels of *Zscan4* associated with *Rif1* depletion might result from alteration of tightly regulated population equilibrium in ESCs by increasing the percentage of *Zscan4*$^+$ cells or from increasing the overall levels of *Zscan4* mRNA.

Rif1 Suppresses Hyper Telomere Recombination to Maintain Telomere Length Homeostasis and Chromosomal Stability

Sporadic *Zscan4* expression in an ESC population is associated with telomere extension by recombination (Zalzman et al., 2010). Early two-cell embryos can activate rapid telomere lengthening through telomere recombination or telomere sister chromatid exchange (T-SCE) (Liu et al., 2007). We confirmed that telomeres were shorter in *Zscan4*$^-$ than in *Zscan4*$^+$ ESCs (Figure 2A). In contrast, average telomere lengths were longer in *Rif1* KD than in control ESCs (Figures 2B and 2C). However, telomere length heterogeneity, telomere loss, and end-to-end chromosomal fusions were pronounced in *Rif1*-depleted ESCs (Figures 2B–2D). *Rif1* KD in other independent ESC lines also led to telomere elongation and telomere signal free-ends indicative of telomere loss, whereas *Zscan4* KD resulted in telomere shortening and loss (Figure S3A). Telomerase activity, estimated by semiquantitative telomeric repeat amplification protocol assay, remained similar between *Rif1* and control KD ESCs or ESCs without transfection manipulation (Figure S3B), suggesting that telomerase activity is unlikely to be responsible for heterogeneous telomere elongation. Instead, a telomerase-independent mechanism of telomere lengthening might be triggered by *Rif1* depletion. Indeed, the frequency of T-SCE was considerably increased in *Rif1* KD ESCs compared to that in control KD ESCs (Figures 2E and 2F). Extremely heterogeneous telomere lengths are associated with increased frequency of T-SCE (Bailey et al., 2004; Londoño-Vallejo et al., 2004). It is interesting that DNA damage signals at telomeres indicated by γH2AX foci (TIFs) (Takai et al., 2003) showed no noticeable differences between *Rif1* and control KD ESCs or between control ESCs and ESCs with *Zscan4* overexpression (Figures S3C and S3D). Analysis of DNA damage at telomeres marked by 53BP1 also showed only low frequency of double-strand telomere damage in *Rif1*-depleted ESCs, like that in control ESCs, in contrast to the high incidence of TIFs found in mitomycin-C-treated MEF that served as feeders (Figures S3E and S3F). These data show that depletion of *Rif1* in ESCs did not increase double-strand breakage at telomeres. However, cell cycle progression, particularly S phase, was impaired in *Rif1*-depleted ESCs (Figures S3G and S3H), which is consistent with the role of *Rif1* in S-phase checkpoint (Silverman et al., 2004). Collectively, *Rif1* is important for maintaining telomere length homeostasis, genomic stability, and cell cycle checkpoint in ESCs by suppression of hyper T-SCE.

Zscan4 KD Rescues Telomere Length Homeostasis and Proliferation of *Rif1*-Depleted ESCs

Hyper telomere recombination induces cell senescence (Hagelstrom et al., 2010). *Zscan4* is critical to elongate telomeres and maintain genomic stability of mouse ESCs (Zalzman et al., 2010). Although other genes located at subtelomeric regions including *Tcstv1* and *Tcstv3* also are upregulated after *Rif1* KD, whether they play a role in regulating telomere length in ESCs remains unclear. We reasoned that aberrantly elevated expression of *Zscan4* following *Rif1* depletion might trigger hyper telomere elongation, leading to disrupted telomere length homeostasis and cell senescence. To test this hypothesis, we performed *Zscan4* KD experiments to rescue phenotypes of stable *Rif1* KD ESCs. Both mRNA and protein level of *Zscan4* in *Rif1*-depleted ESCs following *Zscan4* KD dropped to levels similar to those of control KD ESCs (Figure 3A). ESCs with *Rif1*/*Zscan4*

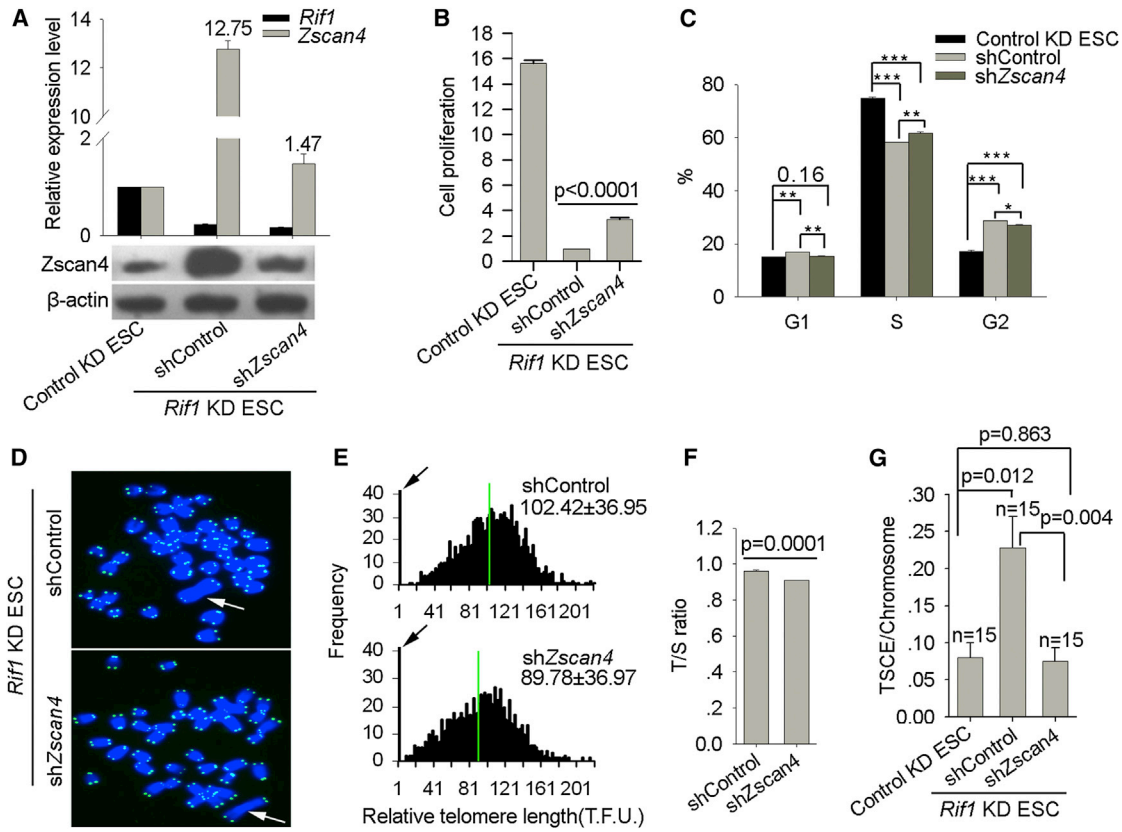

Figure 3. *Zscan4* KD Partially Rescues Cell Proliferation and Shortens Telomeres in *Rif1*-Depleted ESC

(A) Expression levels of *Rif1* and *Zscan4* by qPCR analysis (upper panel) and Zscan4 protein levels by western blot analysis (lower panel) after shZscan4 in *Rif1*-depleted ESCs.

(B) Increased rates of cell proliferation in *Rif1* KD ESC after shZscan4. The fold increase in the cell number of shZscan4 cells was compared with that of shControl cells (arbitrarily set as 1.0).

(C) Cell cycle analysis of *Rif1* KD ESC after shZscan4 treatment.

(D) Telomere specific PNA-FISH image of *Rif1* KD ESC treated with shControl and shZscan4. Arrow, telomere loss and chromosomal fusions.

(E) Distribution histogram of relative telomere length in *Rif1* KD ESCs treated with shControl and shZscan4. Green line indicates median telomere length. Arrows on y axis indicate frequency of telomere loss.

(F) Telomere length shown as relative telomere to single copy gene (T/S) ratio by qPCR analysis.

(G) Decreased frequency of T-SCE per chromosome after shZscan4 in *Rif1*-depleted ESCs, comparable to that of control KD ESCs. Statistical comparison made by Mann-Whitney test.

Error bars indicate mean ± SEM (n = 3). *p < 0.05, **p < 0.01, and ***p < 0.001, compared to controls.

double KD proliferated faster than did *Rif1* KD ESCs, despite rates still slower than those of control ESCs (Figure 3B). Consistently, the cell cycle progression was partially rescued, presumably due to the chromosome fusion and genomic instability already accumulated during long-term culture after *Rif1* depletion (Figure 3C). Furthermore, aberrant telomere elongation was reversed in *Rif1*/*Zscan4* double KD ESCs (Figures 3D–3F). Meanwhile, elevated frequency of T-SCE in *Rif1*-depleted ESCs was reduced, comparable to that of control ESCs following *Zscan4* KD (Figure 3G). As expected, *Zscan4* KD failed to rescue telomere loss and chromosomal fusions that preexisted in *Rif1*-depleted ESCs, which also explains partial rescue of the cell proliferation phenotype (Figures 3D and 3E). Of note, the average of arbitrary telomere fluorescence units (TFUs) indicative of relative telomere lengths in Figure 3E (indicated by "shControl") was larger than that of ES controls shown in Figure 2C. This is probably because the *Rif1* KD ESCs were cultured for additional eight passages, and telomeres of mouse ESCs/induced pluripotent stem cells are known to become elongated with prolonged passage (Marion et al., 2009; Varela et al., 2011; Wang et al., 2012). Nevertheless, these data suggest that excessive expression of *Zscan4* resulting from depletion of *Rif1* mediates cell senescence through aberrant telomere lengthening and heterogeneity accompanied by hyper frequency of T-SCE. Suppression of *Zscan4* is one of major functions of *Rif1* in maintaining telomere length homeostasis of mouse ESCs.

Embryogenesis Defects on *Rif1*-Deficient Background Can Be Rescued by Reducing *Zscan4* Levels

It has been shown that *Rif1*-deficient mice are embryonic lethal mutants (Buonomo et al., 2009). However, the roles of Rif1 at early embryogenesis were not well understood. More important, because Rif1 may be potentially implicated in multiple important biological processes, the significance of Rif1's functions in

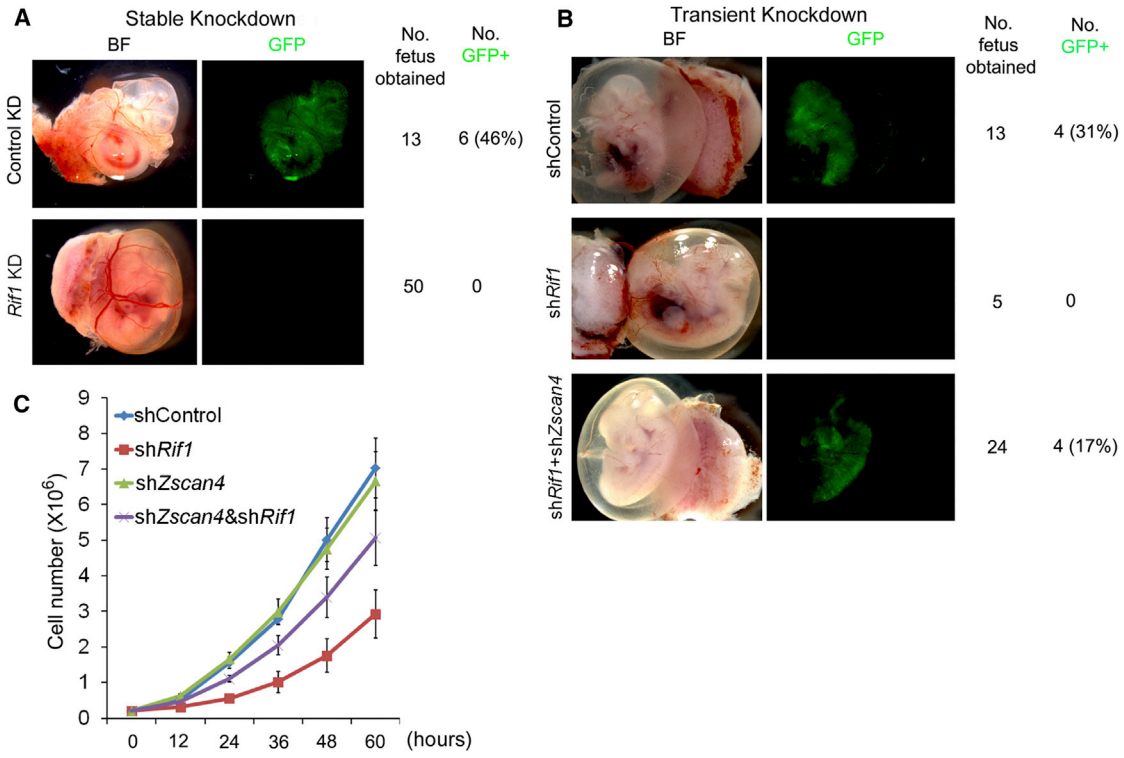

Figure 4. Embryogenesis Defects on *Rif1*-Deficient Backgrounds Are Rescued by *Zscan4* KD

(A) Chimera fetus at E12.5 obtained from blastocyst injection of EGFP-labeled control and stable *Rif1* KD ESCs into albino recipient embryos (number of embryos transferred = 40 and 65, respectively). BF, bright field.

(B) A cohort of transient KD cells labeled with EGFP (shcontrol, sh*Rif1* alone, and sh*Rif1*/*Zscan4*) were generated. Chimera fetus at E12.5 was obtained from injection of this cohort of cells into albino recipient embryos (number of embryos transferred = 30, 22, and 30, respectively).

(C) Growth curves show that *Zscan4* KD significantly rescued the proliferation phenotype caused by short-term *Rif1* depletion. Transient KD cells were seeded (2×10^5 cells per well) 24 hr before counting, and cell number was counted every 12 hr by the TC10 Automated Cell Counter (Bio-Rad).

regulating ESC telomere recombination during early embryogenesis needs to be addressed. We generated chimera mice using GFP-tagged control and *Rif1* KD cell lines and examined chimerism at embryonic day (E)12.5. While control KD ESCs gave rise to 46% (6/13) of chimeric fetus (GFP+) (Figure 4A), *Rif1* KD ESCs failed to contribute to the developing embryos (E12.5) (0/50). Next, we addressed the role of Rif1-mediated telomere recombination in early embryogenesis. We reasoned that, since Zscan4 is a critical downstream effector in Rif1-mediated telomere maintenance pathway, reducing the aberrantly upregulated *Zscan4* expression in *Rif1*-depleted cells may rescue the defects in early embryogenesis. Thus, we generated control KD (shControl) ESCs as well as ESCs in which *Rif1* and *Zscan4* were simultaneously depleted (shRif1+shZscan4) or in which only *Rif1* was depleted (shRif1). To avoid secondary effects potentially arising from prolonged *Rif1* depletion, we immediately used these cells to generate chimeric mice after KD (48–72 hr). As expected, shRif1 ESCs still did not contribute to the developing embryos at E12.5 (0/5; Figure 4B), while shControl ESCs contributed to chimeric fetus normally (31%; 4/13). Notably, shRif1+shZscan4 ESCs gave rise to 17% (4/24) of chimeric fetus that exhibited GFP fluorescence (Figure 4B). In line with these observations, simultaneous depletion of *Rif1* and *Zscan4* appeared to rescue the cell growth phenotypes more efficiently (Figure 4C). These data suggest that reducing excessive *Zscan4* levels could, at least partially, rescue embryogenesis defects associated with *Rif1* deficiency.

Depletion of *Rif1* Influences *Zscan4* Promoter Activity

Rif1 KD resulted in immediate upregulation of *Zscan4* (Figures 1F and 1G; Figures S2F and S2G), but *Zscan4* KD did not cause appreciable changes in the expression of *Rif1* (Figure 5A). We determined whether *Zscan4* promoter activity is affected following *Rif1* KD using the luciferase activity assay. The promoter activity of *Zscan4* dramatically increased following *Rif1* KD but was not influenced by KD of *Zscan4* itself (Figure 5B). We then sought to investigate whether overexpression of *Zscan4* could affect its promoter activity. Zscan4c contains one SCAN-B domain and four zinc finger motifs (Storm et al., 2009), so we designed three expression vectors containing different domains of Zscan4 (Figure 5C). *Zscan4* promoter activity was increased by overexpression of full-length Zscan4 and also by Zscan4-1, which contains the SCAN-B domain. Zscan4-2 with Zinc finger motifs seemed not to alter the reporter activity (Figure 5D). These results demonstrate that the SCAN-B domain is necessary but not sufficient for activation of *Zscan4* promoter activity and that Zinc finger motifs are dispensable for the promoter activity but can complement its activation by the SCAN-B domain.

Furthermore, we divided the promoter of *Zscan4* into nine regions (Figure 5E), with the initiation codon located at +812 base

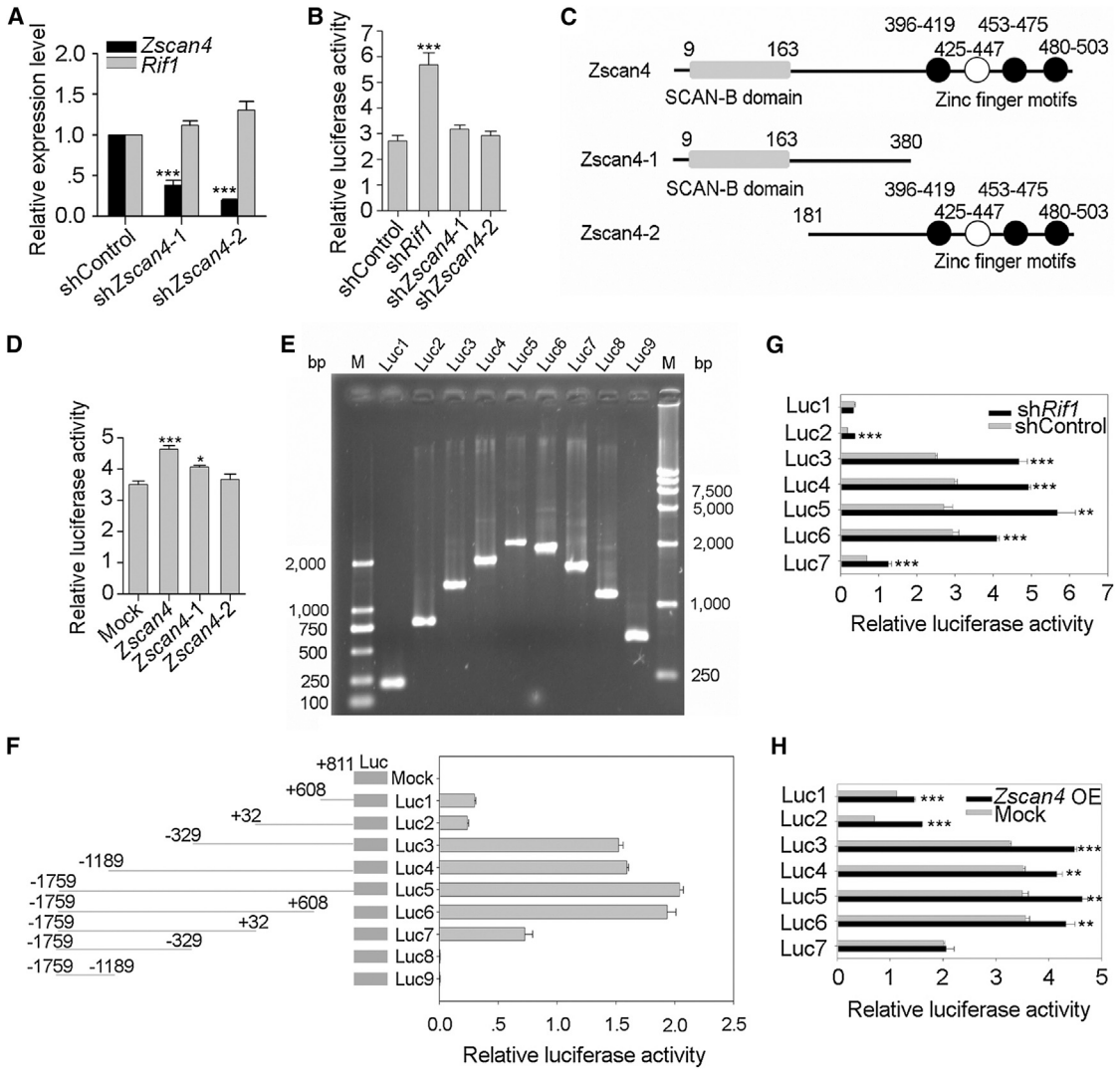

Figure 5. *Rif1* Depletion Results in Increased *Zscan4* Promoter Activity

(A) KD efficiency of *Zscan4* by shRNA for 24 hr by qPCR. *Rif1* level was not influenced by *Zscan4* KD.

(B) Transient *Rif1* KD for 24 hr increases *Zscan4* promoter activity, while *Zscan4* KD does not influence *Zscan4* promoter activity by dual luciferase reporter assay.

(C) Diagram of full length of Zscan4, zinc finger motifs depleted Zscan4-1, and SCAN-B domain depleted Zscan4-2. Filled circles indicates the conserved motif of the Zscan4 gene family, and open circles represent the less conserved motif.

(D) *Zscan4* overexpression for 24 hr increases *Zscan4* promoter activity through its SCAN-B domain.

(E) Agarose gel images of nine fragment regions of the Zscan4 promoter. Luc1, +811 to +608; Luc2, +811 to +32; Luc3, +811 to −329; Luc4, +811 to −1,189; Luc5, +811 to −1,759 (full length of putative Zscan4 promoter); Luc6, +608 to −1,759; Luc7, +32 to −1,759; Luc8, −329 to −1,759; Luc9, −1,189 to −1,759.

(F) Promoter activity of different regions of *Zscan4*. The full-length 2,570 bp of putative *Zscan4* promoter cover regions 2,570 bp upstream to *Zscan4c* translational start codon.

(G and H) Luciferase activity of Luc1-Luc7 24 hr after *Rif1* KD (G) or overexpression (OE) of *Zscan4* (H).

Mean ± SEM (n = 3–4). *p < 0.05, **p < 0.01, and ***p < 0.001, compared to controls or Mock.

pairs (bp) (Zalzman et al., 2010). The promoter activity was low in Luc1/Luc2 but rapidly increased from Luc3 (Figure 5F), suggesting that the core promoter or enhancer of *Zscan4* is located near the Luc3 region. Luc8/9 did not show detectable activity. While Luc1 did not show activity changes, Luc2 showed increased activity resulting from depletion of *Rif1* (Figure 5G). Luc3–Luc6 regions also exhibited increased *Zscan4* promoter activity by *Rif1* KD. Luc7 did not contain Luc2 but also showed increased promoter activity after *Rif1* KD. Similarly, overexpression of *Zscan4* influenced Luc2 at +608 to +811 and at +32 to +608 (Figure 5H). Depletion of *Rif1* results in an increase in *Zscan4* promoter activity. The question was how Rif1 negatively regulates *Zscan4* expression.

Rif1 Depletion Reduces H3K9me3 Enrichment at Heterochromatin

Further analysis of the microarray data identifies that many of the upregulated genes on *Rif1* depletion are located at subtelomeric

sites (Table S3). We hypothesized that Rif1 might function at telomeres or subtelomeres of ESCs at a given time. By immunofluorescence microscopy, Rif1 was located with large clustered and peripheral heterochromatin in a proportion of ESCs and associated with some telomeric repeat binding factor 1 (TRF1) foci, suggestive of localization of Rif1 at telomeric or subtelomeric regions (Figure S4A).

H3K9me3 marks the heterochromatin and plays a critical role in epigenetic silencing thereat (Mikkelsen et al., 2007). *Rif1* KD ESCs exhibited generally reduced H3K9me3 fluorescence intensity by immunofluorescence microscopy (Figures 6A and 6B). Immunoblot analysis also showed that H3K9me3 levels were decreased after *Rif1* KD, but double KD of *Rif1* and *Zscan4* did not change H3K9me3 levels (Figure 6C and Figure S4B). However, H3K27me3 and H3K4me3 levels remained relatively stable following *Rif1* depletion (Figure S4B).

Telomeres and subtelomeres are densely compacted with DNA methylation and histone modifications. Chromatin modifications of telomeres and subtelomeres are important regulators of mammalian telomere lengths (Blasco, 2007). DNA demethylation by treatment with 5-aza-2′-deoxycytidine (5-azaC) caused a mild increase in populations of Zscan4$^+$ cells, as found with flow cytometry analysis of Zscan4-EGFP cells. However, histone demethylation by treatment with inhibitor of histone lysine methyltransferases (BIX-01294) (Kubicek et al., 2007) remarkably increased the population of Zscan4$^+$ cells by 3- to 4-fold (Figures S5A–S5C), supporting the notion that intermittent activation and expression of *Zscan4* could be regulated by histone modifications at subtelomeric heterochromatin. Actually, the *Zscan4* gene is located at the subtelomeric region of chromosome 7, and interestingly, telomerase-deficient ESCs or MEFs with short telomeres also exhibit significantly increased expression of *Zscan4* (Huang et al., 2011) and decreased levels of repressive histones in telomeric and subtelomeric chromatin (Benetti et al., 2007). These data provide further evidence in supporting telomere position effects in mammalian cells (Baur et al., 2001; Koering et al., 2002). Collectively, these data imply that *Zscan4* might be negatively regulated by histone modifications.

Furthermore, we performed the chromatin immunoprecipitation sequencing (ChIP-seq) experiments to investigate the genome-wide distribution of H3K9me3 in *Rif1*-depleted ESCs. Consistent with previous findings (García-Cao et al., 2004; Martens et al., 2005; Mikkelsen et al., 2007), H3K9me3 was enriched at telomeres, subtelomeres, and pericentromeric heterochromatin (Figures 6D–6G). In *Rif1* KD ESCs, H3K9me3 enrichment was significantly reduced in 33% of genomic regions (16,370 of a total 47,947 regions) and increased only in 1% (472 of total 47,947 regions) (Figure 6D; Tables S4 and S5). The ChIP-seq data are corroborated by the immunoblot results, showing similar reduction in H3K9me3 levels following *Rif1* depletion (Figure 6C and Figure S4B). Decreased H3K9me3 level was primarily located in the distal intergenic regions (Figure 6E). The H3K9me3 level was reduced at telomeric repeats in *Rif1* KD ESCs (Figure 6F), and also at a majority of subtelomeric (within 10Mb from telomere ends) and pericentromeric regions (within 10 Mb from centromeres) ($p < 10^{-5}$ versus genome random) (Figure 6G). For example, H3K9me3 levels were substantially reduced at the subtelomeric regions of Chr7 and Chr13 where the *Zscan4* clusters and *Tcstv3* and *Tcstv1* genes are located, respectively (Figures 6H and 6I). Likewise, H3K9me3 levels at pericentromeric regions of Chr6 and at subtelomeres of ChrY declined in *Rif1*-depleted ESCs (Figures 6J and 6K). These data are consistent with upregulation of these genes following stable *Rif1* KD by microarray analysis (Figure S2 and Table S1). The ChIP-seq experiments suggest that Rif1 may indirectly mediate *Zscan4* regulation via histone modifications at the subtelomeres.

Rif1 Regulates *Zscan4* Expression by Stabilizing H3K9 Methylation at Subtelomeric Heterochromatin

The ChIP-seq data suggested a role for Rif1 in regulating local heterochromatic distribution. To test whether Rif1 directly binds to the *Zscan4* loci and subtelomeric heterochromatic regions, we performed ChIP-quantitative PCR (qPCR) using Rif1 antibody and the primers specific for the promoter-proximal regions of *Zscan4c* loci, subtelomeres of chromosome 7, and telomeres. Rif1 indeed bound to six proximal locations upstream to the *Zscan4* promoter, subtelomeres of chromosome 7, and telomeres (Figure 7A). Also, H3K9me3 levels in *Rif1*-depleted cells declined at the same locations (Figure 7B). Consistent with ChIP-seq results (Figure 6H), the ChIP-qPCR data suggest that Rif1 likely plays a direct role in regulating H3K9me3 levels and facilitates epigenetic silencing at the *Zscan4* loci and subtelomeres.

To further elucidate the molecular basis for Rif1 function, we performed coimmunoprecipitation experiments to probe possible interactions between Rif1 and the H3K9 methylation complex. Indeed, Rif1 interacts with the core components of this complex, including Kap1, Suv39h1, heterochromatin protein α, G9a, and Glp (Figure 7C, left). These interactions were specific for the H3K9 methylation machinery, but not for Lsd1 (histone demethylase), Ezh2, or Suz12 (component of the H3K27 methylation machinery). In support, Rif1 was enriched at H3K9me3-, but not H3K27me3- or H3K4me3-containing nucleosomes (Figure 7C, left). Reciprocally, Rif1 could be pulled down by anti-H3K9me3 antibody (Figure 7C, right). These data show that Rif1 selectively interacts with components of the H3K9 methylation complex.

Interestingly, the levels of major H3K9 methyltransferases, Suv39h1, Glp, and G9a—but not the H3K4 or H3K27 modifying enzymes (e.g., Ezh2)—were reduced in *Rif1* KD ESCs (Figure 7D). A previous study demonstrated that the stability of the major H3K9 methyltransferases, such as Setdb1, Suv39h1, and G9a, are dependent on the physical interactions with other noncatalytic components within a H3K9 methylation modification supercomplex (Fritsch et al., 2010). We hypothesized that Rif1 may bridge these interactions and, therefore, regulate the stability of H3K9 methyltransferases. Thus, we used IP/western approaches to interrogate the interactions between H3K9 methylation components in *Rif1*-depleted cells. In these cells, Glp or HP1 pulled a smaller amount of other core components of H3K9 methylation machinery, suggesting that the interactions among those proteins were greatly reduced (Figure 7E). It was notable that 2-fold (2×) *Rif1* KD lysate was used for Glp IP, since its level was mildly reduced in the *Rif1* KD cells. In addition, we also performed a ChIP-qPCR experiment to examine whether Rif1 regulates the occupancy of the H3K9 methylation machinery at its targets. In *Rif1* KD cells, Glp occupancy at the promoter-proximal regions of *Zscan4* and *Dazl* was reduced by 5- to

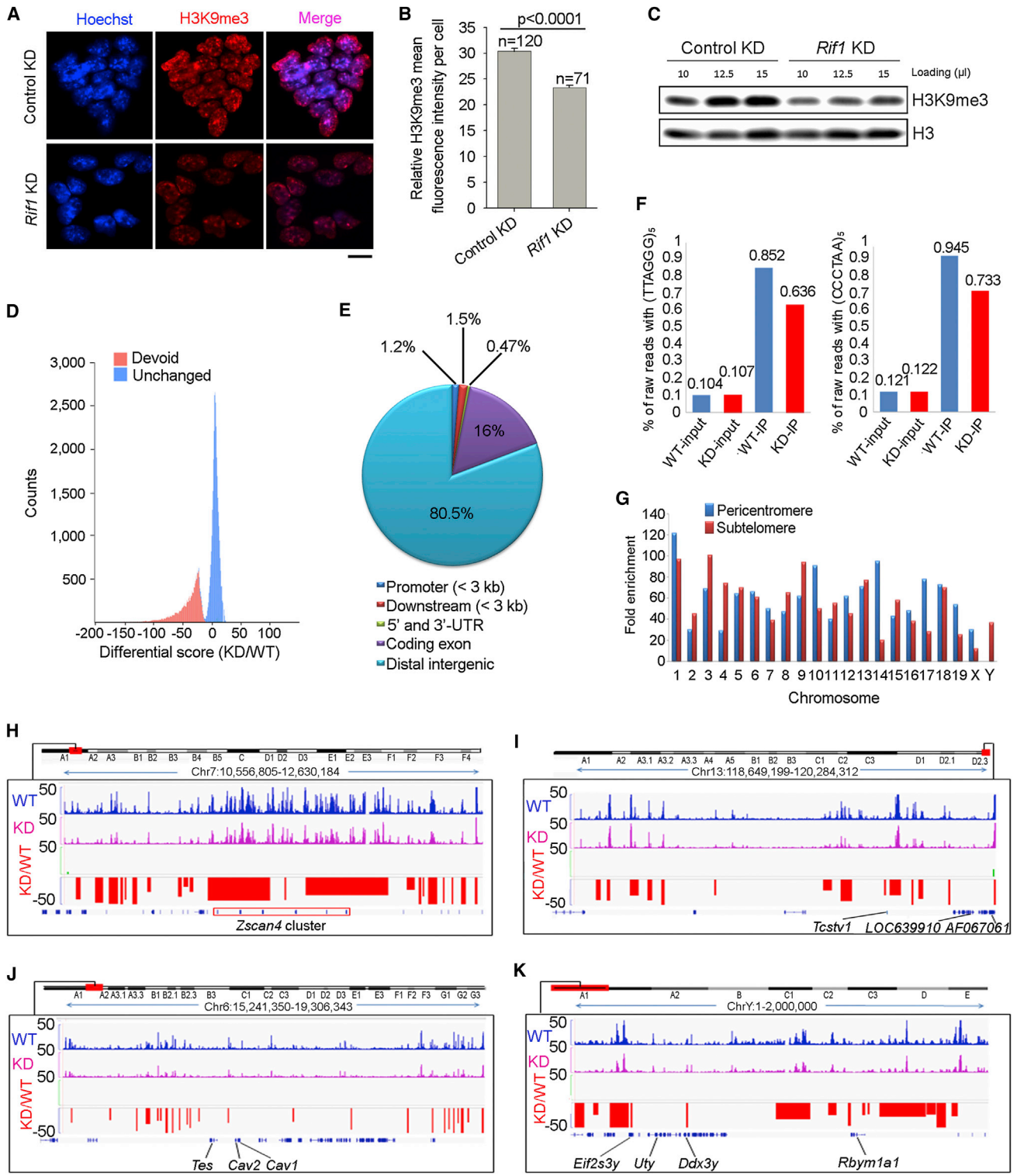

Figure 6. Reduced Genome-wide Enrichment of H3K9me3 by *Rif1* Depletion

(A) Immunofluorescence staining of heterochromatic H3K9me3 (red). Nuclei stained with Hoechst 33342 (blue) show brighter fluorescence signal in the heterochromatin. Scale bar represents 10 μm.

(B) Quantification of relative H3K9me3 fluorescence intensity using ImageJ software. n, number of cells counted. Mean ± SEM (n = 3).

(C) Western blot analysis shows reduced H3K9me3 levels in *Rif1* KD ESCs by loading of progressive dilutions of both control and KD samples. H3, loading control.

(legend continued on next page)

10-fold, compared to that of control KD cells (Figure 7F). The reduced Glp occupancy could result from a mild reduction of the overall level and/or defective recruitment of Glp in *Rif1* KD cells. Taken together, Rif1 stabilizes the H3K9 methylation machinery in ESCs (Figure 7G, left). In *Rif1*-depleted cells, the core components of the H3K9 methylation machinery were greatly disrupted, which leads to reduction of overall protein level and occupancy at the Rif1-regulated genes (Figure 7G, right).

In summary, Rif1 regulates telomere elongation and genomic stability of mouse ESCs. Moreover, Rif1 facilitates epigenetic silencing at subtelomeric heterochromatin, so that Rif1 suppresses the genes located at the subtelomeric regions, including *Zscan4*, *Tcstv3*, and *Tcstv1*. Zscan4 also activates its own promoter, possibly forming a positive feedback loop to increase *Zscan4* expression. Thus, Rif1 plays critical roles in maintaining the transient activation of *Zscan4* in a given ES population, which is essential for telomere maintenance and indefinite self-renewal of ESCs (Figure 7H).

DISCUSSION

We show that high expression levels of *Rif1* in ESCs are required to suppress *Zscan4* overexpression and prevent hyper telomere recombination. High telomerase activity is known to be necessary for telomere length maintenance and continuous proliferation of ESCs. Sporadic expression of *Zscan4* in ESCs is also required for lengthening telomeres via recombination-based mechanisms. Without intermittent activation of *Zscan4*, ESCs lose their ability to proliferate indefinitely (Zalzman et al., 2010). On the contrary, aberrantly high expression levels of *Zscan4* and its continuous expression in ESC populations could cause hyper telomere recombination and cellular senescence over long-term culture (Figure 1). This unique mode of expression suggests a tightly regulated mechanism, but the factors that control *Zscan4* expression remain a mystery. Herein, we show that Rif1 negatively regulates *Zscan4* to prevent its overexpression in ESCs. *Rif1*-depleted ESCs exhibit remarkably high expression levels of *Zscan4*. Moreover, Rif1 modulates epigenetic silencing at subtelomeres including the *Zscan4* locus. This mechanism may restrict *Zscan4* expression to a limited subpopulation of ESCs.

Rif1 has recently been identified as a suppressor of variegation mutants in mice using N-ethyl-N-nitrosourea ENU mutagenesis and whole-exome deep-sequencing approaches (Daxinger et al., 2013), consistent with our finding that Rif1 is a transcriptional repressor (Figures 1F and 1G; Tables S1 and S2). Notably, in *Rif1*-depleted ESCs, a significant portion of upregulated genes are located at pericentromeric regions (e.g., histone cluster genes) and subtelomeric regions of short p arm (e.g., *Zscan4*, *Eif2s3y*, *Uty*, *Ddx3y*, and *Rbym1a1*), where H3K9me3 is enriched. Along this line, we found a consistent, decrease of H3K9me3 modification in the *Rif1*-depleted cells by immunofluorescence microscopy and immunoblotting approaches. This observation was further confirmed by H3K9me3 ChIP-seq approach, showing that H3K9me3 enrichment was reduced at subtelomeres (Figure 6; Tables S4 and S5), including *Zscan4* loci. Rif1 specifically interacts with H3K9 methylation complex, which is critical for the stability of this complex (Figures 7C and 7D). *Rif1* depletion reduces the overall levels of H3K9 methyltransferases, such as G9a, as well as Glp occupancy (Figure 7) at the proximal promoter of *Zscan4*. Taken together, *Rif1* plays an important role in regulation of H3K9me3 and epigenetic transcriptional silencing in ESCs.

In agreement with the fact that Zscan4 is a critical telomere recombination factor, we observed that *Rif1* depletion leads to telomere hyper recombination, elongation, and heterogeneity. These data are substantiated by the experiments showing that double depletion of *Rif1* and *Zscan4* rescues the telomere recombination phenotypes, which suggests that Rif1 maintains telomere length homeostasis via regulation of *Zscan4*. Elevated terminal recombination also may contribute to telomere attrition and genomic instability (Wang et al., 2004). Therefore, it is not surprising that *Rif1*-depleted ESCs exhibit greatly reduced pluripotency both in vitro and in vivo and that simultaneous depletion of *Rif1* and *Zscan4* partially rescues the defective embryogenesis caused by Rif1 deficiency.

Human RIF1 protein is reported to localize at dysfunctional telomeres and telomeric DNA clusters in alternative lengthening of telomere (ALT) cells; however, its function in telomere regulation remains unclear (Silverman et al., 2004). The primary function of mammalian Rif1 in somatic cells appears to be involved in DNA damage responses instead of telomere length regulation (Buonomo et al., 2009; Silverman et al., 2004; Xu and Blackburn, 2004). Here, we demonstrate that Rif1 indeed regulates telomere length homeostasis of ESCs by suppressing excessive Zscan4-mediated telomere recombination. Aberrantly increased T-SCE and heterogeneous telomere elongation via recombination are characteristics of the ALT pathway (Bailey et al., 2004; Londoño-Vallejo et al., 2004). Therefore, this study also may provide insights into tumorigenesis by ALT mechanisms.

(D) Genome-wide distribution of H3K9me3 in *Rif1* KD ESCs compared with control KD (WT) ESCs by ChIP-seq. x axis: differential scores signify the differences in signal intensities of H3K9me3 islands in *Rif1* and control KD cells (R-SEG; see Experimental Procedures). Positive value: enriched in *Rif1* KD ESCs; negative value: devoid in *Rif1* KD ESCs; zero: no change. y axis: occurrence of H3K9me3 islands with the same differential scores.
(E) Annotation of H3K9me3-devoid genomic regions in *Rif1* KD ESCs.
(F) Telomeric H3K9me3 enrichment of *Rif1* KD ESCs is lower than that of control KD (WT) ESCs. ChIP-seq raw reads (before Bowtie alignment) containing $(TTAGGG)_5$ and $(CCCTAA)_5$ represent the H3K9me3 enrichment at telomeres.
(G) H3K9me3-devoid islands at subtelomeric and pericentromeric regions in *Rif1* KD ESCs ($p < 10E-5$ versus random genomic regions). Shown is the enrichment (versus genome random) of such islands on every subtelomeric and pericentromeric regions.
(H–K) Declined H3K9me3 levels at representative subtelomeric and pericentromeric regions. Shown are subtelomeric regions at Chr7, which encode *Zscan4* clusters (H); subtelomeric regions of Chr13, which encode the *Tcstv1*, *LOC639910*, and *AF067061* genes (I); pericentromeric regions of Chr6 (J); and subtelomeric regions of ChrY (K). Blue peaks (WT, top level): H3K9me3 peaks identified by SICER in control KD ES (WT) cells. Cyan peaks (KD, middle level): H3K9me3 peaks in *Rif1* KD ESCs. Red and green peaks (KD/WT, bottom level): Differential scores (KD/WT) denote H3K9me3 signal intensity differences identified by R-SEG (see Experimental Procedures).
See also Figures S4 and S5.

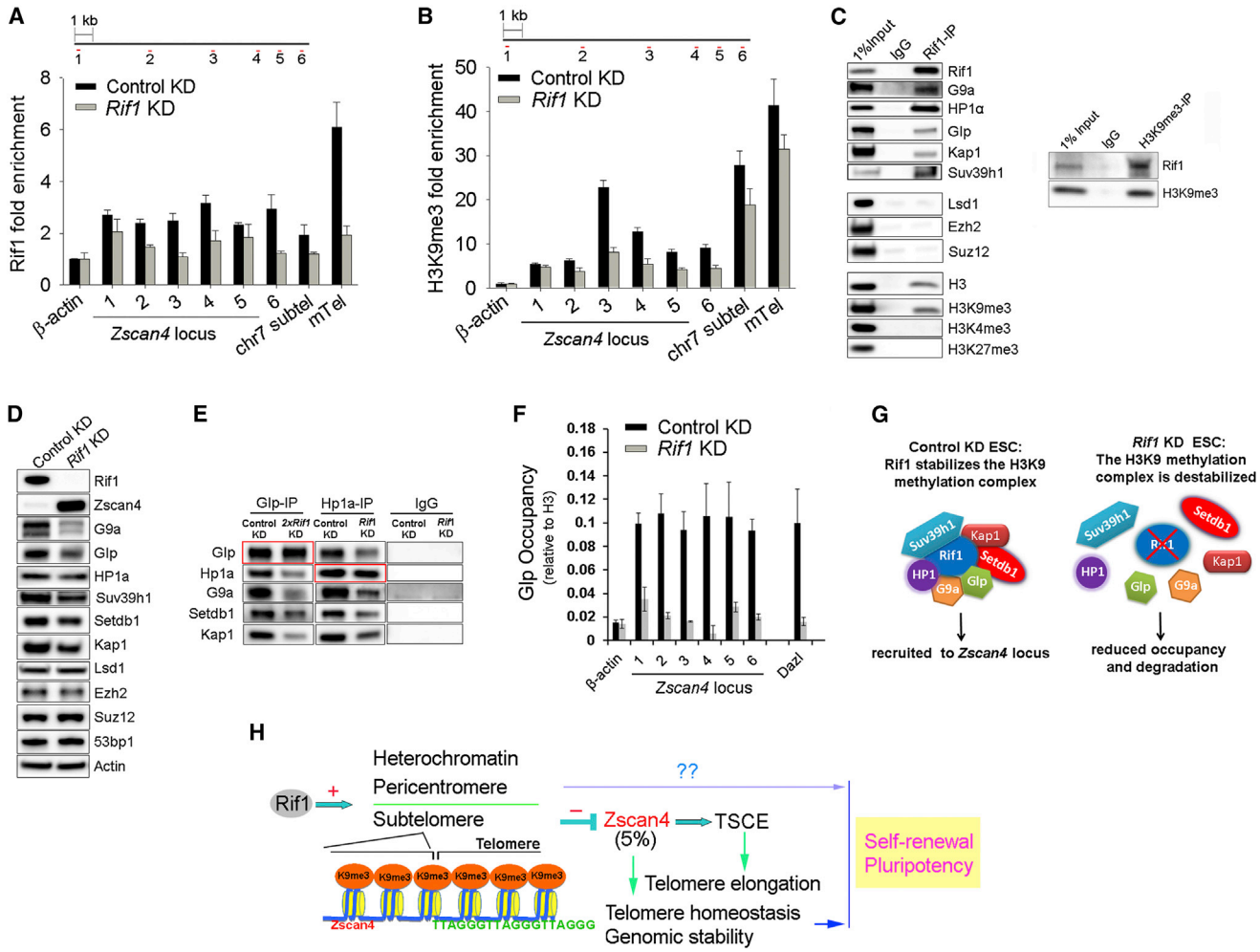

Figure 7. *Rif1* Modulates H3K9 Methylation Machinery to Regulate *Zscan4* Expression

(A) ChIP-qPCR analysis of Rif1 occupancy at six proximal regions of *Zscan4c* promoter, subtelomere of chr7, and telomeres. Relative fold enrichment was normalized to H3 ChIP signals at the same regions, and the β-actin locus served as negative controls. Mean ± SD from three independent assays.

(B) ChIP-qPCR analysis of H3K9me3 occupancy at the same locations using normalization methods and primers indicated in (A). Mean ± SD from three independent assays.

(C) Rif1 interacting proteins were immunoprecipitated and resolved on 4%–20% gradient gel. IgG, pre-immune rabbit IgG, which served as negative control.

(D) Nuclear extracts from control KD and *Rif1* KD ESCs were analyzed by western blotting using the indicated antibodies.

(E) The IP-western approach demonstrated the critical role for Rif1 in stabilizing H3K9 methyltransferase complexes. Since the global levels of Glp were reduced in *Rif1* KD cells, twice the amount (2×) of Glp-IP samples from the *Rif1* KD cells was used in these experiments. Under these conditions, equal amounts of Glp or Hp1α were pulled down from control or *Rif1* KD cells (red boxes). However, their interactions with each other or with other components of the H3K9 methylation complex, such as G9a, Setdb1, or Kap1, were much reduced.

(F) ChIP-qPCR assays showed that Glp occupancy at the *Zscan4* locus (P1-P6) was greatly reduced in the *Rif1*-depleted cells (5- to 10-fold). Glp signals were normalized to H3 ChIP signals. β-actin locus and *Dazl* locus served as negative and positive controls, respectively. Mean ± SD from three independent assays.

(G) A schematic of the molecular functions of Rif1 based on our findings. Left: In WT ESC, Rif1 stabilizes the H3K9 methylation complex and recruits this complex to downstream gene targets, such as *Zscan4*. Right: in the absence of Rif1 protein, the H3K9 methylation complex fails to assemble appropriately, resulting in two parallel phenotypes. First, several key components are partially degraded. Second, the complex is less efficiently recruited to the *Zscan4* locus, leading to excessive *Zscan4* expression.

(H) A model for *Rif1* function and epigenetic regulation of *Zscan4* expression and self-renewal of ESCs.

EXPERIMENTAL PROCEDURES

Mouse ESCs

Animals were cared for and treated according to guidelines set by U.S. National Research Council, and the use of mice for this research was approved by the Nankai Animal Care and Use Committee. Mouse ESCs are detailed in Supplemental Experimental Procedures.

Generation of *Rif1* KD ESCs by shRNA

After an initial test on RNAi efficiency using four different shRNA sequences against *Rif1* mRNA, *Rif1* shRNA3 and control shRNA were used for the following experiments if not otherwise mentioned (Supplemental Experimental Procedures). The sequences were cloned into pSIREN-RetroQ (Clontech), and the resultant vectors were transfected into F1 or N12 ESCs with Lipofectamine 2000 according to the manufacturer's instructions.

Long-term Rif1 KD ESCs were then selected with 1.5 μg/ml puromycin for 2 weeks.

Microarray Analysis of *Rif1* KD ESCs

J1 ESCs were transfected with control shRNA and *Rif1* shRNA using lipofectamine 2000. Forty-eight hours after transfection, cells were collected for global gene expression analysis using Affymetrix mouse genome 430 2.0 array. Stable *Rif1* KD F1 ESCs at passage 16 were used for long-term gene expression chip microarray using Affymetrix mouse genome 430 2.0 array. Hybridization, staining, and scanning of the chips was performed as outlined in the Affymetrix technical manual. Hybridized arrays were scanned with a Gene Array Scanner (Affymetrix). Significantly different genes were identified using a one-class unpaired significance analysis of microarrays (Tusher et al., 2001) and fold change. Only probe sets showing a false discovery rate (FDR) less than 5% and absolute fold change greater than 2.0 were retained in the final list. Hierarchical clustering was performed with the aforementioned differentially expressed genes using cluster software (version 3) and by applied mean centering and normalization of genes and arrays before average linkage clustering.

Telomere Quantitative Fluorescence In Situ Hybridization

Telomere length and function (telomere integrity and chromosome stability) was estimated by quantitative fluorescence in situ hybridization (QFISH). Cells were incubated with 0.5 μg/ml nocodazole for 1.5 hr to enrich cells at metaphases. Chromosome spreads were made by a routine method. Metaphase-enriched cells were exposed to hypotonic treatment with 75 mM KCl solution, fixed with methanol: glacial acetic acid (3:1) and spread onto clean slides. Telomere FISH and quantification were performed as described previously (Herrera et al., 1999; Poon et al., 1999), except for fluorescein isothiocyanate (FITC)-labeled (CCCTAA) peptide nucleic acid (PNA) probe (Panagene) used in this study. Telomeres were denatured at 80°C for 3 min and hybridized with telomere-specific PNA probe (0.5 μg/ml). Chromosomes were counterstained with 0.5 μg/ml DAPI. Fluorescence from chromosomes and telomeres was digitally imaged on a Zeiss microscope with FITC/DAPI filters, using AxioCam and AxioVision software 4.6. For quantitative measurement of telomere length, telomere fluorescence intensity was integrated using the TFL-TELO program (a gift kindly provided by P. Lansdorp, Terry Fox Laboratory), and calibrated using standard fluorescence beads.

Telomere Chromatid Orientation-Fluorescence In Situ Hybridization

Strand-specific chromatid orientation-fluorescence in situ hybridization (CO-FISH) was performed according to Bailey et al. (2004), with minor modification. Subconfluent cells were incubated with BrdU. Nocodazole was added for 1.5 hr prior to cell harvest, and metaphase spreads were prepared by standard cytogenetic method as described earlier. Chromosome preparations were stained with Hoechst 33258 (0.5 μg/ml), incubated in 2× SSC (Invitrogen) for 20 min and exposed to 365 nm UV light (Stratalinker 1800 UV irradiator) for 40 min. The BrdU-substituted DNA was digested with Exonuclease III (Promega). The slides were then dehydrated through cold ethanol series and air dried. PNA-FISH was performed with Fluorescein-OO-$(CCCTAA)_3$ (Bio-Synthesis). Slides were hybridized, washed, dehydrated, mounted, and counterstained with VectaShield antifade medium (Vector), containing 0.1 μg/ml DAPI. Digital images were captured using a CCD camera on a Zeiss AxioImager Z1 microscope equipped with Metasystems Isis software.

ChIP-Seq, ChIP-qPCR, and Data Analysis

ChIP and data analysis were performed as described elsewhere (Hunter et al., 2012; Martinez et al., 2010; Maze et al., 2011; Mikkelsen et al., 2007; Rowe et al., 2010), using primary antibodies to Rif1 (ab13422, Abcam) or H3K9me3 (ab8898, Abcam). Normal rabbit immunoglobulin G (IgG) (Santa Cruz, sc-2027) served as control. Briefly, control KD and *Rif1* KD mouse ESCs (3×10^7) were fixed with freshly prepared 1% paraformaldehyde for 10 min at room temperature. Cells were harvested, and their nuclei were extracted, lysed, and sonicated. DNA fragments were then enriched by immunoprecipitation with 10 μg H3K9me3 antibody (Abcam, ab8898) for ChIP-seq. The eluted protein:DNA complex was reverse-crosslinked at 65°C overnight. DNA was recovered with a MiniElute column (QIAGEN) after Proteinase and RNase A treatment. Approximately 100 ng of each ChIP DNA and its parental genomic DNA (Input) were subjected to a 50 bp single-end library construction, and cluster generation and Illumina HiSeq 2000 sequencing were performed at the Yale Stem Cell Center Sequencing Core Facility. The output sequencing tags were filtered and preanalyzed with the standard ELAND workflow to obtain the fastq data file. Sequence reads were mapped to mm9 (NCBI 37) using Bowtie (Langmead et al., 2009), with default settings allowing one single mismatch. Peak calling (versus input) was performed by SICER (Zang et al., 2009) using the following cutoffs: FDR < 0.0001, window size = 300 bp, and gap size = 600 bp. To identify genomic regions with differential H3K9me3 enrichment following *Rif1* KD, we used the R-SEG algorithm (Song and Smith, 2011), with slight modifications to the default settings (bin size of 5 kb; posterior probability of each bin: > 0.95). We used a three-state hidden Markov model for segmentation of the genome (devoid, unchanged, and increased).

In ChIP-qPCR experiments, the ChIP-enriched DNA was analyzed by real-time PCR using primers for *Zscan4c* loci, subtelomeres, telomeres, or *Dazl*. β-actin served as negative control, and relative fold changes were normalized to pan-H3 levels.

Immunofluorescence-Telomere FISH

The immunofluorescence (IF)-FISH method was performed based on an established protocol (Sfeir et al., 2010). Briefly, cells were grown on gelatin-treated coverslips and fixed with 2% paraformaldehyde for 10 min at room temperature. Cells were then blocked in blocking solution (1 mg/ml BSA, 3% goat serum, 0.1% Triton X-100, and 1 mM EDTA, pH 8.0) and incubated with anti-53BP1 antibody (Abcam, ab36823) in blocking solution. Secondary antibody against rabbit IgG was labeled with Alexa Fluor 568 (Invitrogen). Cells were fixed again with 2% paraformaldehyde for 5 min, and FISH was performed with FITC-$(TTAGGG)_3$ PNA telomere probe (Panagene) as described earlier. DNA was counterstained with 0.5 μg/ml Hoechst 33342 in Vectashield mounting medium. Fluorescence was detected and imaged using a Zeiss fluorescence microscope and using the same exposure time for each group.

Mouse Embryogenesis Assay

Control KD and *Rif1* KD stable ESCs were transfected with *Ef1α*-EGFP reporter vector and selected with G418, and EGFP-positive cells were picked for further expansion and chimera production by microinjection. Stable *Ef1α*-EGFP control and *Rif1* KD ESCs were then injected into albino ICR blastocysts, using a Piezo injector, and transferred into uterine horns of surrogate mice 2.5 days postcoitum. For embryo imaging, chimera fetus was collected at E12.5 and imaged under stereo fluorescence microscopy (Leica, M165FC). For short-term *Rif1* KD and *Rif1*/*Zscan4* double KD, shControl, sh*Rif1*, and sh*Zscan4* retrovirus were packaged by transfection of the indicated RNAi vectors into PlatE packaging cells. *Ef1α*-EGFP F1 ESCs were infected with shControl, sh*Rif1*, or sh*Rif1*/sh*Zscan4* double KD retrovirus for 48 hr. Infected ESCs were injected into ICR blastocysts as described earlier.

Statistical Analysis

Percentages were transformed using arcsine transformation. Percentage of transformed data and other numbers were analyzed by ANOVA, and means were compared by Fisher's protected least significant difference (PLSD) using the StatView software from SAS Institute. Significant differences were defined as $p < 0.05$, 0.01, or lower.

ACCESSION NUMBERS

The ChIP-seq data (accession number GSE54947) and gene expression array data sets (accession number GSE55129) have been deposited in the Gene Expression Omnibus database (http://www.ncbi.nlm.nih.gov/geo).

SUPPLEMENTAL INFORMATION

Supplemental Information includes five figures, Supplemental Experimental Procedures, and five tables and can be found with this article online at http://dx.doi.org/10.1016/j.devcel.2014.03.004.

AUTHOR CONTRIBUTIONS

J.D. prepared and wrote the manuscript; J.D., Y.L., and N.L. performed experiments and analyzed the data; M.C., M.O., X.Y., C.M., L.W., L.L.W.,Y.Y., J.Y., B.Z., F.W., and Z.L. performed experiments; X.P., Z.Y., T.W., and L.C. analyzed the data; Y.L. revised the manuscript; D.L.K. and S.G. analyzed the data and revised the manuscript; A.X. and L.L. designed the experiments and wrote and revised the manuscript.

ACKNOWLEDGMENTS

We thank Minoru Ko for providing Zscan4 antibody, Christina Glytsou for help on CO-FISH, Xinglong Zhou for fluorescence-activated cell sorting (FACS), Peter Lansdorp for the TFL-TELO software, Zhe Liu for H3K9me3 antibody (Upstate, 07-442), Jun Zhou for pCMV-Tag2B and pSIREN-RetroQ vector, and Mark Bartlam for reading the manuscript. This work was supported by the MOST National Key Basic Research Program (2011CBA01002, 2012CB911202); National Natural Science Foundation of China (31271587); Tianjin Science & Technology Planned Program (12JCZDJC24800); intramural Biomedical Research Foundation, Academy of Athens funding to S.G.; and a Howard Temin Award (K99/R00 NIH/NCI 5R00CA131560 to A.X.).

Received: April 5, 2013
Revised: November 18, 2013
Accepted: March 11, 2014
Published: April 14, 2014

REFERENCES

Adams, I.R., and McLaren, A. (2004). Identification and characterisation of mRif1: a mouse telomere-associated protein highly expressed in germ cells and embryo-derived pluripotent stem cells. Dev. Dyn. *229*, 733–744.

Bailey, S.M., Brenneman, M.A., and Goodwin, E.H. (2004). Frequent recombination in telomeric DNA may extend the proliferative life of telomerase-negative cells. Nucleic Acids Res. *32*, 3743–3751.

Baur, J.A., Zou, Y., Shay, J.W., and Wright, W.E. (2001). Telomere position effect in human cells. Science *292*, 2075–2077.

Benetti, R., García-Cao, M., and Blasco, M.A. (2007). Telomere length regulates the epigenetic status of mammalian telomeres and subtelomeres. Nat. Genet. *39*, 243–250.

Blasco, M.A. (2007). The epigenetic regulation of mammalian telomeres. Nat. Rev. Genet. *8*, 299–309.

Bringold, F., and Serrano, M. (2000). Tumor suppressors and oncogenes in cellular senescence. Exp. Gerontol. *35*, 317–329.

Buonomo, S.B., Wu, Y., Ferguson, D., and de Lange, T. (2009). Mammalian Rif1 contributes to replication stress survival and homology-directed repair. J. Cell Biol. *187*, 385–398.

Callen, E., Di Virgilio, M., Kruhlak, M.J., Nieto-Soler, M., Wong, N., Chen, H.T., Faryabi, R.B., Polato, F., Santos, M., Starnes, L.M., et al. (2013). 53BP1 mediates productive and mutagenic DNA repair through distinct phosphoprotein interactions. Cell *153*, 1266–1280.

Chapman, J.R., Barral, P., Vannier, J.B., Borel, V., Steger, M., Tomas-Loba, A., Sartori, A.A., Adams, I.R., Batista, F.D., and Boulton, S.J. (2013). RIF1 is essential for 53BP1-dependent nonhomologous end joining and suppression of DNA double-strand break resection. Mol. Cell *49*, 858–871.

Cornacchia, D., Dileep, V., Quivy, J.P., Foti, R., Tili, F., Santarella-Mellwig, R., Antony, C., Almouzni, G., Gilbert, D.M., and Buonomo, S.B. (2012). Mouse Rif1 is a key regulator of the replication-timing programme in mammalian cells. EMBO J. *31*, 3678–3690.

Daxinger, L., Harten, S.K., Oey, H., Epp, T., Isbel, L., Huang, E., Whitelaw, N., Apedaile, A., Sorolla, A., Yong, J., et al. (2013). An ENU mutagenesis screen identifies novel and known genes involved in epigenetic processes in the mouse. Genome Biol. *14*, R96.

Di Virgilio, M., Callen, E., Yamane, A., Zhang, W., Jankovic, M., Gitlin, A.D., Feldhahn, N., Resch, W., Oliveira, T.Y., Chait, B.T., et al. (2013). Rif1 prevents resection of DNA breaks and promotes immunoglobulin class switching. Science *339*, 711–715.

Escribano-Díaz, C., Orthwein, A., Fradet-Turcotte, A., Xing, M., Young, J.T., Tkáč, J., Cook, M.A., Rosebrock, A.P., Munro, M., Canny, M.D., et al. (2013). A cell cycle-dependent regulatory circuit composed of 53BP1-RIF1 and BRCA1-CtIP controls DNA repair pathway choice. Mol. Cell *49*, 872–883.

Falco, G., Lee, S.L., Stanghellini, I., Bassey, U.C., Hamatani, T., and Ko, M.S. (2007). Zscan4: a novel gene expressed exclusively in late 2-cell embryos and embryonic stem cells. Dev. Biol. *307*, 539–550.

Fritsch, L., Robin, P., Mathieu, J.R., Souidi, M., Hinaux, H., Rougeulle, C., Harel-Bellan, A., Ameyar-Zazoua, M., and Ait-Si-Ali, S. (2010). A subset of the histone H3 lysine 9 methyltransferases Suv39h1, G9a, GLP, and SETDB1 participate in a multimeric complex. Mol. Cell *37*, 46–56.

García-Cao, M., O'Sullivan, R., Peters, A.H., Jenuwein, T., and Blasco, M.A. (2004). Epigenetic regulation of telomere length in mammalian cells by the Suv39h1 and Suv39h2 histone methyltransferases. Nat. Genet. *36*, 94–99.

Hagelstrom, R.T., Blagoev, K.B., Niedernhofer, L.J., Goodwin, E.H., and Bailey, S.M. (2010). Hyper telomere recombination accelerates replicative senescence and may promote premature aging. Proc. Natl. Acad. Sci. USA *107*, 15768–15773.

Hardy, C.F., Sussel, L., and Shore, D. (1992). A RAP1-interacting protein involved in transcriptional silencing and telomere length regulation. Genes Dev. *6*, 801–814.

Herbig, U., Jobling, W.A., Chen, B.P., Chen, D.J., and Sedivy, J.M. (2004). Telomere shortening triggers senescence of human cells through a pathway involving ATM, p53, and p21(CIP1), but not p16(INK4a). Mol. Cell *14*, 501–513.

Herrera, E., Samper, E., Martín-Caballero, J., Flores, J.M., Lee, H.W., and Blasco, M.A. (1999). Disease states associated with telomerase deficiency appear earlier in mice with short telomeres. EMBO J. *18*, 2950–2960.

Hu, G., Kim, J., Xu, Q., Leng, Y., Orkin, S.H., and Elledge, S.J. (2009). A genome-wide RNAi screen identifies a new transcriptional module required for self-renewal. Genes Dev. *23*, 837–848.

Huang, J., Wang, F., Okuka, M., Liu, N., Ji, G., Ye, X., Zuo, B., Li, M., Liang, P., Ge, W.W., et al. (2011). Association of telomere length with authentic pluripotency of ES/iPS cells. Cell Res. *21*, 779–792.

Hunter, R.G., Murakami, G., Dewell, S., Seligsohn, M., Baker, M.E., Datson, N.A., McEwen, B.S., and Pfaff, D.W. (2012). Acute stress and hippocampal histone H3 lysine 9 trimethylation, a retrotransposon silencing response. Proc. Natl. Acad. Sci. USA *109*, 17657–17662.

Iglesias, N., Redon, S., Pfeiffer, V., Dees, M., Lingner, J., and Luke, B. (2011). Subtelomeric repetitive elements determine TERRA regulation by Rap1/Rif and Rap1/Sir complexes in yeast. EMBO Rep. *12*, 587–593.

Koering, C.E., Pollice, A., Zibella, M.P., Bauwens, S., Puisieux, A., Brunori, M., Brun, C., Martins, L., Sabatier, L., Pulitzer, J.F., and Gilson, E. (2002). Human telomeric position effect is determined by chromosomal context and telomeric chromatin integrity. EMBO Rep. *3*, 1055–1061.

Kubicek, S., O'Sullivan, R.J., August, E.M., Hickey, E.R., Zhang, Q., Teodoro, M.L., Rea, S., Mechtler, K., Kowalski, J.A., Homon, C.A., et al. (2007). Reversal of H3K9me2 by a small-molecule inhibitor for the G9a histone methyltransferase. Mol. Cell *25*, 473–481.

Langmead, B., Trapnell, C., Pop, M., and Salzberg, S.L. (2009). Ultrafast and memory-efficient alignment of short DNA sequences to the human genome. Genome Biol. *10*, R25.

Levy, D.L., and Blackburn, E.H. (2004). Counting of Rif1p and Rif2p on Saccharomyces cerevisiae telomeres regulates telomere length. Mol. Cell. Biol. *24*, 10857–10867.

Liu, L., Bailey, S.M., Okuka, M., Muñoz, P., Li, C., Zhou, L., Wu, C., Czerwiec, E., Sandler, L., Seyfang, A., et al. (2007). Telomere lengthening early in development. Nat. Cell Biol. *9*, 1436–1441.

Loh, Y.H., Wu, Q., Chew, J.L., Vega, V.B., Zhang, W., Chen, X., Bourque, G., George, J., Leong, B., Liu, J., et al. (2006). The Oct4 and Nanog transcription network regulates pluripotency in mouse embryonic stem cells. Nat. Genet. *38*, 431–440.

Londoño-Vallejo, J.A., Der-Sarkissian, H., Cazes, L., Bacchetti, S., and Reddel, R.R. (2004). Alternative lengthening of telomeres is characterized by high rates of telomeric exchange. Cancer Res. *64*, 2324–2327.

Marion, R.M., Strati, K., Li, H., Tejera, A., Schoeftner, S., Ortega, S., Serrano, M., and Blasco, M.A. (2009). Telomeres acquire embryonic stem cell characteristics in induced pluripotent stem cells. Cell Stem Cell *4*, 141–154.

Martens, J.H., O'Sullivan, R.J., Braunschweig, U., Opravil, S., Radolf, M., Steinlein, P., and Jenuwein, T. (2005). The profile of repeat-associated histone lysine methylation states in the mouse epigenome. EMBO J. *24*, 800–812.

Martinez, P., Thanasoula, M., Carlos, A.R., Gómez-López, G., Tejera, A.M., Schoeftner, S., Dominguez, O., Pisano, D.G., Tarsounas, M., and Blasco, M.A. (2010). Mammalian Rap1 controls telomere function and gene expression through binding to telomeric and extratelomeric sites. Nat. Cell Biol. *12*, 768–780.

Maze, I., Feng, J., Wilkinson, M.B., Sun, H., Shen, L., and Nestler, E.J. (2011). Cocaine dynamically regulates heterochromatin and repetitive element unsilencing in nucleus accumbens. Proc. Natl. Acad. Sci. USA *108*, 3035–3040.

Mikkelsen, T.S., Ku, M., Jaffe, D.B., Issac, B., Lieberman, E., Giannoukos, G., Alvarez, P., Brockman, W., Kim, T.K., Koche, R.P., et al. (2007). Genome-wide maps of chromatin state in pluripotent and lineage-committed cells. Nature *448*, 553–560.

Poon, S.S., Martens, U.M., Ward, R.K., and Lansdorp, P.M. (1999). Telomere length measurements using digital fluorescence microscopy. Cytometry *36*, 267–278.

Rowe, H.M., Jakobsson, J., Mesnard, D., Rougemont, J., Reynard, S., Aktas, T., Maillard, P.V., Layard-Liesching, H., Verp, S., Marquis, J., et al. (2010). KAP1 controls endogenous retroviruses in embryonic stem cells. Nature *463*, 237–240.

Sfeir, A., Kabir, S., van Overbeek, M., Celli, G.B., and de Lange, T. (2010). Loss of Rap1 induces telomere recombination in the absence of NHEJ or a DNA damage signal. Science *327*, 1657–1661.

Shi, T., Bunker, R.D., Mattarocci, S., Ribeyre, C., Faty, M., Gut, H., Scrima, A., Rass, U., Rubin, S.M., Shore, D., and Thomä, N.H. (2013). Rif1 and Rif2 shape telomere function and architecture through multivalent Rap1 interactions. Cell *153*, 1340–1353.

Silverman, J., Takai, H., Buonomo, S.B., Eisenhaber, F., and de Lange, T. (2004). Human Rif1, ortholog of a yeast telomeric protein, is regulated by ATM and 53BP1 and functions in the S-phase checkpoint. Genes Dev. *18*, 2108–2119.

Song, Q., and Smith, A.D. (2011). Identifying dispersed epigenomic domains from ChIP-seq data. Bioinformatics *27*, 870–871.

Storm, M.P., Kumpfmueller, B., Thompson, B., Kolde, R., Vilo, J., Hummel, O., Schulz, H., and Welham, M.J. (2009). Characterization of the phosphoinositide 3-kinase-dependent transcriptome in murine embryonic stem cells: identification of novel regulators of pluripotency. Stem Cells *27*, 764–775.

Takai, H., Smogorzewska, A., and de Lange, T. (2003). DNA damage foci at dysfunctional telomeres. Curr. Biol. *13*, 1549–1556.

Teixeira, M.T., Arneric, M., Sperisen, P., and Lingner, J. (2004). Telomere length homeostasis is achieved via a switch between telomerase- extendible and -nonextendible states. Cell *117*, 323–335.

Tusher, V.G., Tibshirani, R., and Chu, G. (2001). Significance analysis of microarrays applied to the ionizing radiation response. Proc. Natl. Acad. Sci. USA *98*, 5116–5121.

Varela, E., Schneider, R.P., Ortega, S., and Blasco, M.A. (2011). Different telomere-length dynamics at the inner cell mass versus established embryonic stem (ES) cells. Proc. Natl. Acad. Sci. USA *108*, 15207–15212.

Wang, R.C., Smogorzewska, A., and de Lange, T. (2004). Homologous recombination generates T-loop-sized deletions at human telomeres. Cell *119*, 355–368.

Wang, J., Rao, S., Chu, J., Shen, X., Levasseur, D.N., Theunissen, T.W., and Orkin, S.H. (2006). A protein interaction network for pluripotency of embryonic stem cells. Nature *444*, 364–368.

Wang, H., Zhao, A., Chen, L., Zhong, X., Liao, J., Gao, M., Cai, M., Lee, D.H., Li, J., Chowdhury, D., et al. (2009). Human RIF1 encodes an anti-apoptotic factor required for DNA repair. Carcinogenesis *30*, 1314–1319.

Wang, F., Yin, Y., Ye, X., Liu, K., Zhu, H., Wang, L., Chiourea, M., Okuka, M., Ji, G., Dan, J., et al. (2012). Molecular insights into the heterogeneity of telomere reprogramming in induced pluripotent stem cells. Cell Res. *22*, 757–768.

Xu, L., and Blackburn, E.H. (2004). Human Rif1 protein binds aberrant telomeres and aligns along anaphase midzone microtubules. J. Cell Biol. *167*, 819–830.

Yamazaki, S., Ishii, A., Kanoh, Y., Oda, M., Nishito, Y., and Masai, H. (2012). Rif1 regulates the replication timing domains on the human genome. EMBO J. *31*, 3667–3677.

Zalzman, M., Falco, G., Sharova, L.V., Nishiyama, A., Thomas, M., Lee, S.L., Stagg, C.A., Hoang, H.G., Yang, H.T., Indig, F.E., et al. (2010). Zscan4 regulates telomere elongation and genomic stability in ES cells. Nature *464*, 858–863.

Zang, C., Schones, D.E., Zeng, C., Cui, K., Zhao, K., and Peng, W. (2009). A clustering approach for identification of enriched domains from histone modification ChIP-seq data. Bioinformatics *25*, 1952–1958.

Zhang, W., Walker, E., Tamplin, O.J., Rossant, J., Stanford, W.L., and Hughes, T.R. (2006). Zfp206 regulates ES cell gene expression and differentiation. Nucleic Acids Res. *34*, 4780–4790.

Zimmermann, M., Lottersberger, F., Buonomo, S.B., Sfeir, A., and de Lange, T. (2013). 53BP1 regulates DSB repair using Rif1 to control 5′ end resection. Science *339*, 700–704.